Electrochimica Acta 283 (2018) 1178–1187

Contents lists available at ScienceDirect

Electrochimica Acta

journal homepage: www.elsevier.com/locate/electacta

Layer-by-layer assembly of iron oxide-decorated few-layer graphene/PANI:PSS composite films for high performance supercapacitors operating in neutral aqueous electrolytes

Gonzalo E. Fenoy [a, b], Benoit Van der Schueren [c], Juliana Scotto [a, d], Fouzia Boulmedais [e], Marcelo R. Ceolín [a], Sylvie Bégin-Colin [f], Dominique Bégin [c], Waldemar A. Marmisollé [a, **], Omar Azzaroni [a, *]

[a] Instituto de Investigaciones Fisicoquímicas Teóricas y Aplicadas (INIFTA), Departamento de Química, Facultad de Ciencias Exactas, Universidad Nacional de La Plata (UNLP), CONICET. 64 and 113, La Plata, 1900, Argentina
[b] Instituto de Investigación e Ingeniería Ambiental, Universidad Nacional de San Martín, 25 de mayo y Francia, 1 piso, 1650, Buenos Aires, Argentina
[c] Université de Strasbourg, CNRS, Institut de chimie et procédés pour l'énergie, l'environnement et la santé, UMR 7515, 67087, Strasbourg, France
[d] Instituto de Ciencias de la Salud, Universidad Nacional Arturo Jauretche, Av. Calchaquí 6200, Florencio Varela, Buenos Aires, Argentina
[e] Université de Strasbourg, CNRS, Institut Charles Sadron UPR 22, 67034, Strasbourg, France
[f] Université de Strasbourg, CNRS, Institut de physique et chimie des matériaux de Strasbourg, 67034, Strasbourg, France

ARTICLE INFO

Article history:
Received 27 May 2018
Received in revised form
13 July 2018
Accepted 14 July 2018
Available online 17 July 2018

Keywords:
Supercapacitors
2D materials
Graphene
Conducting polymers
Energy storage

ABSTRACT

The layer-by-layer assembly of polyaniline-PSS (PANI:PSS) complexes and iron oxide nanoparticles-decorated few-layer graphene (Fe-FLG) from aqueous dispersions, yielding an electrode material with excellent electrochemical capacitive performance in simple neutral aqueous electrolyte is presented. The simple dip-coating procedure allows the effective incorporation of both materials and the control of the film nanoarchitectonics. The resulting composite coating was characterized by XPS and Raman spectroscopies. A linear dependence of the capacitance on the film mass indicates that both building blocks are efficiently (and electrochemically) connected within the films. The electrochemical performance of the film-coated electrodes was tested in both acidic (0.1 M HCl) and neutral (0.1 M KCl) aqueous electrolytes. Electrodes constituted of 15 self-assembled bilayers showed the best performance with a high capacitance of 768.6 F g^{-1} and 659.2 F g^{-1} in 0.1 M HCl and 0.1 M KCl, respectively, at the current density of 1 A g^{-1}. Moreover, a high stability to continuous cycling was observed, even in aqueous neutral solution (86% capacitance retention after 1600 cycles at 3 A g^{-1}). This ternary material then constitutes a promising candidate for the construction of environmentally friendly supercapacitors.

© 2018 Published by Elsevier Ltd.

1. Introduction

Nanoarchitectonics refers to the rational design and construction of nanostructures into functional materials with control at the nanoscale [1–3]. Within nanoarchitectonics, the integration of hybrid polymer–inorganic nanoarchitectures at solid interfaces has attracted considerable attention in many electrochemical applications. In particular, the precise control of the film architecture and the effective integration of the different building blocks are crucial aspects in the construction of electrochemical devices for energy storage applications [4,5]. In this sense, the layer-by-layer (LbL) assembly becomes an enabling methodology facilitating the integration of polymers and nanomaterials in a controlled fashion, avoiding nanomaterials aggregation and producing an intimate contact of the film components [6,7].

Supercapacitors (SCs) are electrochemical devices able to store charge by a nanometer-scale charge separation between the electrolyte and the electrode material by two main mechanisms: the electrochemical double-layer capacitance (EDLC) and redox capacitance [8]. The SCs performance depends on the electrode material and its nanoarchitecture, especially if composites or

* Corresponding author.
** Corresponding author.
E-mail addresses: wmarmi@inifta.unlp.edu.ar (W.A. Marmisollé), azzaroni@inifta.unlp.edu.ar (O. Azzaroni).

https://doi.org/10.1016/j.electacta.2018.07.085
0013-4686/© 2018 Published by Elsevier Ltd.

hybrid materials are employed [9,10]. Beyond the electrode composition, an increase of the energy density can be achieved by using organic electrolytes (increasing the operating voltage), but with a concomitant loss of capacitance and power densities and other disadvantages as their toxic nature and polluting production. On the contrary, neutral aqueous electrolytes appear as a non-corrosive good alternative due to a combination of different factors, as its high conductivity, low-cost, environmental-friendliness [11].

Few-layer graphene (FLG) refers to a 2D-structure formed by a small number (typically 2–10) of stacked graphene layers. These carbon nanomaterials have become versatile building blocks in the construction of electrochemical devices due to their unique electrical, mechanical, and chemical properties [12–16]. The main charge storage mechanism operating in these materials is the double-layer capacitance, but the global capacitance can be strongly increased by incorporating other electroactive materials, such as metal oxides [17,18] or conducting polymers (CPs) [19–21].

Polyaniline (PANI) has been one of the most studied CPs for supercapacitors applications owing to its inexpensive simple synthesis and high stability and electroactivity in acidic solutions and the possibility of storing charge by its reversible electrochemical transformations (redox capacitance) [22–24]. However, the swelling and shrinkage during the doping/dedoping process and the poor electroactivity at pH 7 limit the storage performance and cyclability of PANI-based SCs in neutral aqueous electrolytes.

Particularly, the complementary properties of carbon nanomaterials and PANI have recently promoted a great interest in producing composites to be applied in charge storage devices [25–27]. A synergistic effect can be attained by the high redox switching rate of PANI and the mechanical stability and good electronic conductivity of carbon nanomaterials [22,28]. Even an increase in the electronic conductivity of PANI composites in neutral solutions can be achieved by a doping effect within the assemblies [29–31]. However, the control of composition and architecture of the hybrid PANI/carbon nanomaterial coating remains as a keystone for transforming the nanocomposite into an electrochemically active film [32,33].

On the other hand, the combination of inorganic nanomaterials, carbon nanomaterials and conducting polymers has been demonstrated as an efficient way of merging the positive features of each material [34–36]. As an example, Pardieu et al. [37] developed a hybrid LbL assembly of PEDOT:PSS and Fe_3O_4 NPs-modified FLG with good capacitance and cyclability, whereas Li et al. [38] presented a free-standing composite paper of MnO_2 nanoflakes/PANI nanorods on rGO with even higher gravimetric capacitance in Na_2SO_3 solutions. Other systems comprising the integration of Fe_3O_4, PANI and carbon nanomaterials have been reported to present a good capacitive performance in acidic solutions [39,40]. Table 1 presents a detailed comparison of the capacitive performance of some hybrid coatings.

Within this scenario, in this work we present a hybrid electroactive material formed by the LbL assembly of PANI:PSS complexes and iron oxide nanoparticles-coated FLG by dip-coating from aqueous dispersions, yielding an electrochemically stable electrode material. The capacitance and coating mass result linear on the number of deposition cycles, indicating a homogenous film growing-up and highly connected nanoarchitecture. The film-coated electrodes present high capacitance retention when going from highly acidic to neutral KCl solution, due to the enhanced electroactivity of PANI. Moreover, charge-discharge curves showed good cycling stability even in KCl solution, reinforcing its utility as electroactive material in environmentally friendly aqueous supercapacitors.

2. Experimental section

2.1. Chemicals

Aniline, Ammonium Persulfate (APS), Polyethylenimine (PEI) (50% in H_2O, Mw~750 kDa), Poly (sodium 4-styrene sulfonate) (PSS) (Mw~70 kDa) were purchased from Sigma-Aldrich. Sulfuric Acid, Hydrochloric Acid and Potassium Chloride were purchased from Anedra. (1-Hexadecyl)trimethyl-ammonium bromide 98% (CTAB) and 1-octadecene (90%) were purchased from Alfa Aesar. Expanded graphite was purchased from Carbone Lorraine, Iron (II) stearate (9% of iron) and sodium stearate (tech. grad.) were purchased from Strem Chemicals. Oleic acid was purchased from VWR Chemicals.

All chemicals were employed as received except for Aniline, which was vacuum distilled. All solutions were prepared with Milli-Q water (18.2 MΩ cm).

2.2. Fe-FLG synthesis

The FLG was obtained by ultrasonication of expanded graphite in the presence of CTAB as surfactant. Briefly, 10 mg of CTAB was dissolved in 200 mL of water and 200 mg of expanded graphite was added. Probe sonication was performed during 2 h at 120 W of power. The material was filtered and dried overnight at 60 °C.

The synthesis method used to produce the iron oxide-modified FLG was the thermal decomposition of iron stearate complex in a high boiling point solvent in presence of FLG [41]. In more detail, 200 mg of FLG was firstly dispersed in a solution of 1.44 g of iron stearate (II), 0.184 g of oleic acid and 0.706 g of sodium oleate in 15 mL 1-octadecene in a sonication bath during 15 min. The solution was heated to 120 °C in order to dry the material, and 15 min later the system was closed with a cooling condenser and heated up to 290 °C for 2 h. After the reaction, the Fe-FLG was cleaned with chloroform by centrifugation 5 times and filtered on a Buchner flask. The material was dried overnight at 60 °C. Finally, 25 mg of Fe-FLG was dispersed in 25 mL of CTAB solution (1 g/50 mL) for 1 min probe sonication (120 W of power) in order to be used in the LbL assembly process.

2.3. PANI:PSS complex synthesis

Firstly, a 5 mM aniline solution in 0.5 M HCl was prepared in a 40 mL falcon tube. The solution was stirred for 10 min and then PSS was added to achieve a concentration of 5 mM in monomer units. Finally, solid APS was added to reach a 5 mM concentration and the solution was stirred for 3 h. For the LbL building-up, a 1/10 dilution of this stock solution was employed.

2.4. Layer-by-Layer assembly process

Before starting the assembly process, the Au electrodes were cleaned with soft basic piranha solution ($1NH_4OH:1H_2O_2:7H_2O$). The LbL assembly was started by immersing the substrates in a 1 mg mL^{-1} PEI solution for 10 min [42]. After that, a rinsing with Milli-Q water for 5 min was performed. Then, the substrates were alternatively dipped in a PANI:PSS 1/10 in 0.5 M HCl solution for 10 min with a wash step in 0.5 M HCl for 5 min and in a CTAB-exfoliated Fe-FLG solution with a rinsing with Milli-Q water for 5 min. This constituted a single bilayer, so the n times repetition of that process yielded a $(PANI:PSS/Fe\text{-}FLG)_n$ assembly.

2.5. TEM

Transmission electron microscopy was carried out on a JEOL 2100F with a voltage 200 kV and a point resolution of 0.2 nm. To

Table 1
Supercapacitor performance comparison between this study and others.

Method	Electrolyte (three electrode cell)	C_{SP} (F g^{-1})	Cycling stability	Reference
Spin-coating layer-by-layer of PEDOT:PSS and raspberry-like Fe_3O_4 NPs-modified few-layer graphene	0.5 M Na_2SO_3 while N_2 bubbling	153 F g^{-1} at 0.1 A g^{-1}	114% after 1600 cycles	[37] Pardieu et al. *J. Mater. Chem. A*, **2015**, 3 (45), 22877–22885
Free-standing composite paper of MnO_2 nanoflakes/polyaniline nanorods hybrid nanostructures on reduced graphene oxide	1 M Na_2SO_3	636.5 F g^{-1} at 1 A g^{-1}	85% after 10000 cycles	[38] Li et al. *J. Mater. Chem. A*, **2015**, 3 (33), 17165–17171
Layer-by-layer assembly of graphene oxide and Fe_3O_4 NPs	1 M NaCl	151 F g^{-1} at 0.9 A g^{-1}	85% after 1000 cycles	[61] Khoh et al. *Colloids Surfaces A Physicochem. Eng. Asp.* **2013**, 436, 104–112
Stainless steel/multiwalled carbon nanotubes/polyaniline electrode	Physiological electrolyte (PBS, pH 7.4, 0.1 M KH_2PO_4 + 0.1 M Na_2HPO_4 + 0.1 M NaCl)	401 F g^{-1} at 1.4 A g^{-1}	90% after 2000 cycles	[62] Ammam et al. *Chem. Commun.* **2012**, 48 (14), 2036.
Graphite foam/PANI/SnS_2 by electrodeposition	2 M Na_2SO_4	300 F g^{-1} at 1 A g^{-1}	73% after 5000 cycles	[63] Wang et al. *2D Mater.* 5 (2018) 031005.
Core-shell polypyrrole/polyaniline composite electrode	1 M KCl	291 F g^{-1} at 3 A g^{-1}	Not reported	[64] Mi et al. *J. Power Sources* **2008**, 176 (1), 403–409
	1 M H_2SO_4	416 F g^{-1} at 3 A g^{-1}		
Thin film layer-by-layer assembly of graphene oxide and polyaniline	1 M H_2SO_4	375.2 F g^{-1} at 0.5 A g^{-1}	90.7% after 500 cycles	[65] Lee et al. *J. Mater. Chem.* **2012**, 22 (39), 21092
Layer-by-layer assembly of graphene oxide and polyaniline on polystyrene microsphere followed by the removal of the polystyrene template	1 M H_2SO_4	381 F g^{-1} at 4 A g^{-1}	83% after 1000 cycles	[66] Luo et al. *Electrochim. Acta* 2015, 173, 184–192
Ternary 3D graphene-Fe_3O_4-Polyaniline	1 M H_2SO_4	486.5 F g^{-1} at 1 A g^{-1}	52.1% after 2000 cycles	[39] Mezgebe et al. *Mater. Today Energy* **2017**, 5, 164–172
Ternary rGO/Fe_3O_4/PANI composite	0.5 M H_3PO_4	631.7 F g^{-1} at 1 A g^{-1}	78% after 5000 cycles	[67] Mondal et al. *J. Phys. Chem. C* **2017**, 121 (14), 7573–7583
Layer-by-layer assembly of iron-modified graphene and PANI:PSS complex	0.1 M KCl	659.2 F g^{-1} at 1 A g^{-1}	86% after 1600 cycles	*Our study*
	0.1 M HCl	768.6 F g^{-1} at 1 A g^{-1}	84% after 1600 cycles	

prepare the simple, the powder was dispersed in ethanol by ultrasonication and a drop of the solution was then deposited on a copper grid covered with a carbon membrane.

2.6. XRD

X-ray diffraction measurements were performed on a Bruker D8 Advance with a source of copper and a LynxEye detector in the 20°–80° (2θ) range with a scan step of 0.03°.

2.7. DLS and zeta potential

A 1/10 in 0.5 M HCl PANI:PSS diluted solution (the same used for the LbL assembly process) was used for the dynamic light scattering (DLS) and zeta potential measurements. DLS measurements were carried out with a ZetaSizer Nano (Nano ZSizer-ZEN3600, Malvern, U.K.) at 25 °C. The zeta potential was determined from the electrophoretic mobility measured by laser Doppler velocimetry with the same equipment. The Smoluchowski approximation of the Henry equation was employed for calculations. Measurements were performed in triplicate using disposable capillary cells (DTS 1061 1070, Malvern) at 25 °C with a drive cell voltage of 30 V and employing the monomodal analysis method.

2.8. TGA

Thermogravimetric Analysis (TGA) was carried out on a Q500 Automatic Sample Processor (TA Instruments). Before the analysis, the Fe-FLG was dried at 60 °C for 5 h. For the runs, the sample was heated from 25 to 900 °C at a rate of 20 °C min^{-1} under nitrogen gas purge at 90 mL min^{-1}.

2.9. XPS

The X-ray photoelectron spectroscopy (XPS) measurements were carried out in an ultrahigh vacuum (UHV) spectrometer equipped with a VSW Class WA hemispherical electron analyzer. A dual anode Al Kα X-ray source (1486.6 eV) was used as incident radiation.

2.10. QCM

The quartz crystal microbalance measurements were carried out on the QCM-E1 (Gothenburg, Sweden) equipped with a quartz crystal with gold. The fundamental oscillation frequency of this quartz oscillator is about 5 MHz. This apparatus allows the frequency and dissipation shifts at 5, 15, 25 and 35 MHz to be monitored. The LbL assembly process was performed ex-situ in a homemade Teflon cell by exposing only the gold surface zone of the sensor to the different solutions. After a certain number of bilayers were assembled, the film was dried with N_2. Four different measurements were performed in dry state by mounting and demounting the crystal. As the fundamental frequency and the overtones are superimposed, the changes in frequency were transformed into mass deposited per unit area upon use of the Sauerbrey equation.

2.11. Raman spectroscopy

Raman spectra were acquired using a LabRAM ARAMIS confocal microscope spectrometer equipped with a CCD detector. A 532 nm laser was used as excitation source (100 mW -YAG-with Laser Quantum MPC600 PSU).

2.12. Electrochemical measurements

Electrochemical measurements were carried out with a Gamry Reference 600 potentiostat. A three-electrode Teflon-lined cell was used, with a capacity of 2 mL. The counter electrode used was a Pt wire and the reference electrode used was a Ag/AgCl (3 M NaCl) electrode. All the potentials presented here are referred to this electrode. Gold electrodes were prepared by sputtering on glass plates. A thin layer of Ti was previously deposited on glass substrates to improve the adhesion.

3. Results and discussion

3.1. Fe-FLG and PANI:PSS complex characterization

The grafting of the iron nanostructures onto the FLG was performed by using the solvothermal synthesis method. In order to investigate the crystalline structure of the modified-FLG, X-ray diffraction measurements were performed. The XRD pattern in Fig. 1(A) shows reflection peaks at 30.1°, 35.4°, 43.1°, 57.1°, and 62.6° corresponding to Miller indices (220), (311), (400), (511), and (440) of magnetite phase, respectively. Moreover, the spectrum shows the appearance of two peaks at 26.5° and 54.9°, ascribed as the (002) and (004) reflections of the hexagonal crystalline structure of graphite. This result confirms the incorporation of iron nanostructures onto the exfoliated FLG and the presence of a crystalline phase [37,43].

Moreover, TGA was used determine the amount of iron oxide in the Fe-FLG structures. The major weight losses occur in the range of 400–700 °C (Fig. S1), ascribed as the release of CO and CO_2 from the oxidation of graphene nanosheets. Assuming that the final residues are the iron oxide nanostructures, the iron oxide content results about 22% of the material [18,37].

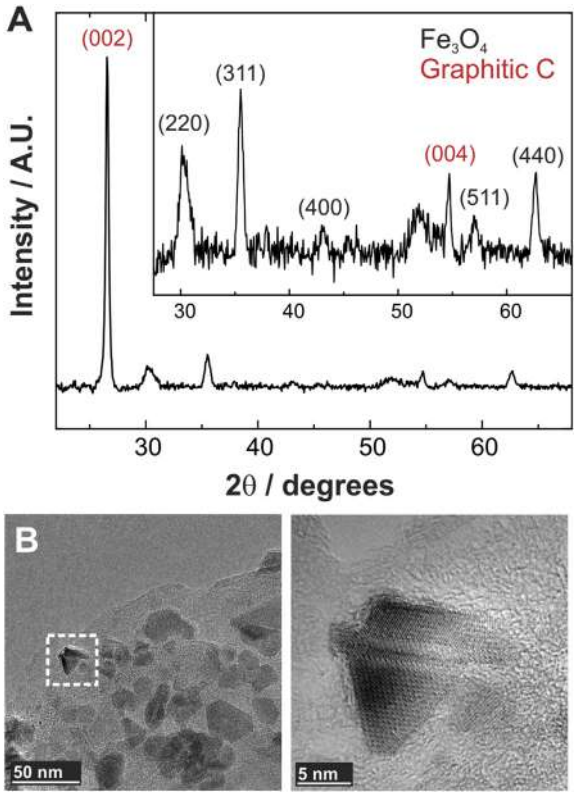

Fig. 1. XRD pattern (A) and TEM images of Fe-FLG (B).

TEM images were taken to explore the morphology of the iron oxide-modified FLG (Fig. 1 (B)). The iron nanostructures randomly decorate the graphene sheets and show a size range between 5 and 10 nm. Moreover, the iron nanostructures remain attached to the FLG after probe sonication, which indicates a strong interaction between both materials. Typically, FLG up to 10 layers was obtained [37,43,44].

In the last years, Raman spectroscopy has emerged as one of the most versatile tools for studying the properties of graphene-related materials. From the number of layers to the presence of functional groups and the doping state, several features of graphene can be studied employing this technique [45]. Herein, Raman measurements were performed to characterize each material, and also to confirm their presence in the LbL assemblies. The Fe-FLG spectrum shows the features of magnetite and graphene; the peak located at 662 cm^{-1} is ascribed as the symmetric stretching of oxygen atoms along the Fe–O bonds (A_{1g}) [46–48]. Considering the graphene zone of the spectrum, the D, G and 2D bands can be observed at 1310 cm^{-1}, 1580 cm^{-1} and 2710 cm^{-1}, respectively. The first band requires the presence of defects for its activation and the I_D/I_G ratio can be used for the evaluation of the degree of disorder/defects present in the graphene-like material. In this case, the I_D/I_G proportion is 0.14, which allow concluding that the exfoliation process for obtaining the graphene and the incorporation of iron nanostructures results in a low proportion of defects in the final material. Furthermore, the low proportion of defects would explain the good electroactivity of the assemblies (the spectrum is presented together with that of the LbL assembly, see below).

The synthesis of PANI:PSS complex involved the PSS-templated oxidative polymerization in acidic solution. This method allows obtaining a negatively charged well-dispersed complex with good electroactivity in neutral solutions. Regarding the PANI:PSS characterization, Fig. 2(A) shows the Raman spectrum of the PANI:PSS complexes deposited onto Au substrate. The characteristic peaks of C–H bending in the quinoid and benzenic ring appear at 810 cm^{-1} and 1170 cm^{-1}, respectively. The peak at 1255 cm^{-1} corresponds to the C–N stretching mode of the polaronic units. The vibration of the semiquinone radical appears at 1340 cm^{-1}. The bands at 1486 cm^{-1} and 1586 cm^{-1} correspond to C=N stretching and C=C stretching of the quinoid ring, respectively. On the other hand, the peaks appearing at 1030 cm^{-1} and 1600 cm^{-1} correspond to the $-SO_3$ moiety of PSS [49,50].

Moreover, dynamic light scattering and zeta potential measurements were performed in order to measure the size and stability of the PANI:PSS dispersion. Fig. 2(B) shows the volume distribution of size obtained from DLS measurement. The size determined for the particles was 47 ± 17 nm and the zeta potential -40 ± 3 mV. The complexes exhibit narrow particle size and its elevated charge in suspension indicates high dispersion stability and allowed them to be easily incorporated in LbL assemblies by dip-coating.

3.2. Layer-by-Layer assembly process

The LbL technique was used to effectively incorporate both materials into electrochemically connected films from aqueous solutions. In Scheme 1, a representation of the LbL assembly process is shown.

Dry-state QCM measurements were performed in order to quantify the mass deposited in each assembly step and use it later for calculating the specific capacitance. Fig. 3(A) shows the changes in the deposited mass as increasing the bilayers number. It can be seen that after 3 bilayers, the growth is linear, indicating that almost the same amount of material is deposited in each LbL cycle. The same linear increase was observed for the peak current in cyclic

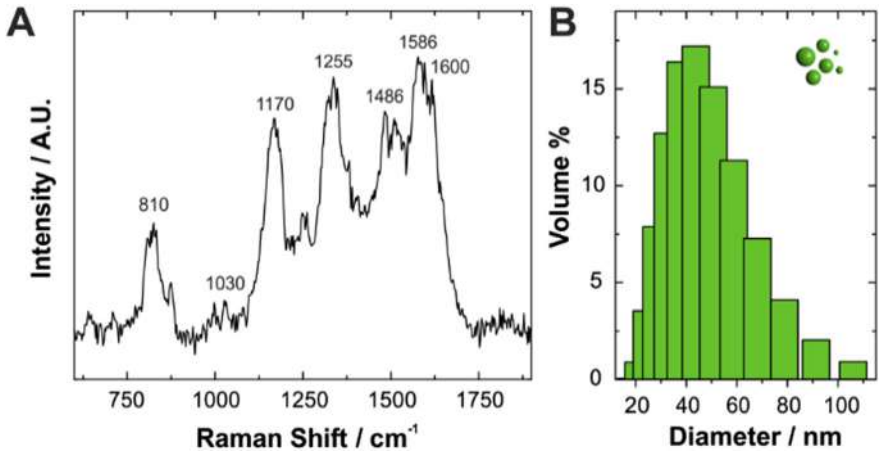

Fig. 2. Raman spectrum (A) and volume size distribution measured by DLS (B) of PANI:PSS complexes.

voltammetry measurements (see below), assessing the excellent integration of the building blocks into a homogeneous coating material.

Fig. 3(B) shows the Raman spectrum of the 9-bilayers assembly. The A_{1g} band of the Fe-FLG appears at 662 cm^{-1}, the C—H bending of the benzenoid ring of PANI:PSS at 1170 cm^{-1}, and the D, G and 2D band of graphene at 1350 cm^{-1}, 1580 cm^{-1} and 2710 cm^{-1}, respectively. This result allows confirming the effective incorporation of both hybrid materials in the LbL assemblies. Detailed descriptions of the Raman spectra of PANI:PSS and Fe-FLG were given in previous sections.

In order to gain further information about the presence of the two components in the LbL assemblies, XPS measurements of a 21 bilayers assembly was performed. The spectra belonging to S2p, C1s, N1s and Fe2p are showed in Fig. 3(C). In the S2p spectrum the signals appear at about 168 eV and can be fitted to a set of two bands at 167.5 and 168.7 eV, assigned to $S2p_{3/2}$ and $S2p_{1/2}$ respectively, corresponding to the sulfonate moiety in PSS [42]. An integrated area ratio of 0.5 was employed for taking into account the degeneration of these levels (fwhm = 1.3 eV). The C1s spectrum shows the presence of three components appearing at 285.0, 285.9 and 286.7 eV. They are assigned to C—C/C═C, C—N/C═N and C—N^+/C═N^+, respectively (fwhm = 1.4 eV) [38,51]. The absence of any oxidized carbon signal accounts also for the low defect level in the graphene-like material incorporated to the assembly, which is consistent with the Raman results. In the case of the N1s spectrum, the peaks appearing at 398.8, 399.5, 400.6 and 402.4 eV are assigned as = N-, −NH−/−NH_2, −$NH.^+$- and −NR_3^+. The first three components correspond to PANI and the last one appears due to the surfactant presence in the assembly (fwhm = 1.7 eV) [52,53]. Finally, the Fe2p spectrum with two signals at 710.6 and 724.5 eV confirms the presence of the iron NPs-modified graphene in the assembly [43,54].

On the other hand, in Fig. 3(D) TEM images of a 6 bilayers assembly are presented. The images show the presence of well dispersed Fe-FLG into the films.

3.3. Electrochemical performance

The incorporation of Fe NPs onto graphene has been reported to improve the capacitance of graphene-like materials [17,18]. To test this idea, cyclic voltammetry measurements of assemblies of PANI:PSS and Fe-FLG or FLG without any grafting were performed. After comparison of the voltammetric results, it can be concluded that the assemblies containing Fe-FLG present improved electrochemical response in both acidic and neutral solutions (Fig. S2). Furthermore, by comparing assemblies having the same number of bilayers, the capacitance is clearly increased in the case of Fe oxide modified-FLG.

It is well-known that the electroactivity of PANI is strongly dependent on the pH of the electrolyte and it is greatly weakened in solutions with pH higher than 3. Therefore, its use in applications operating at neutral pH, such as biosensors and neutral medium supercapacitors is limited. In order to surpass this problem, some authors have employed PANI synthesized in presence of polyanions (such as PSS), yielding complexes electroactive in both acidic and neutral media [55,56]. Following this idea, we made use of the LbL technique for building-up an acidic and neutral media electroactive assembly by alternating PANI:PSS and Fe-FLG layers.

In Fig. 4(A) the cyclic voltammograms at different scan rates in

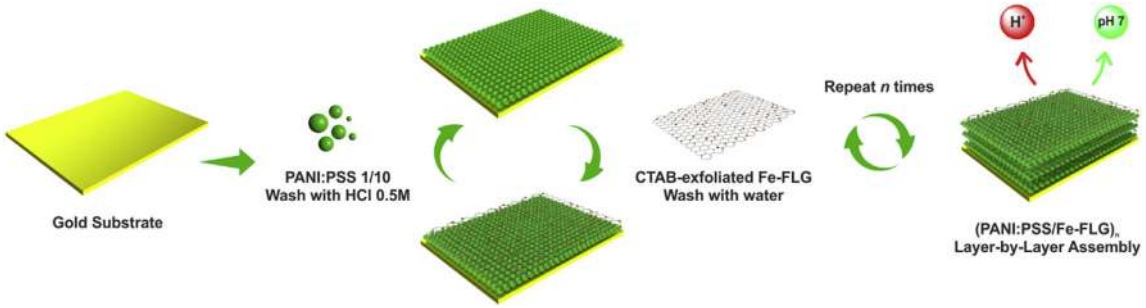

Scheme 1. Representation of the Layer-by-Layer assembly process. In a first step, a layer of PEI is deposited onto the Au substrate.

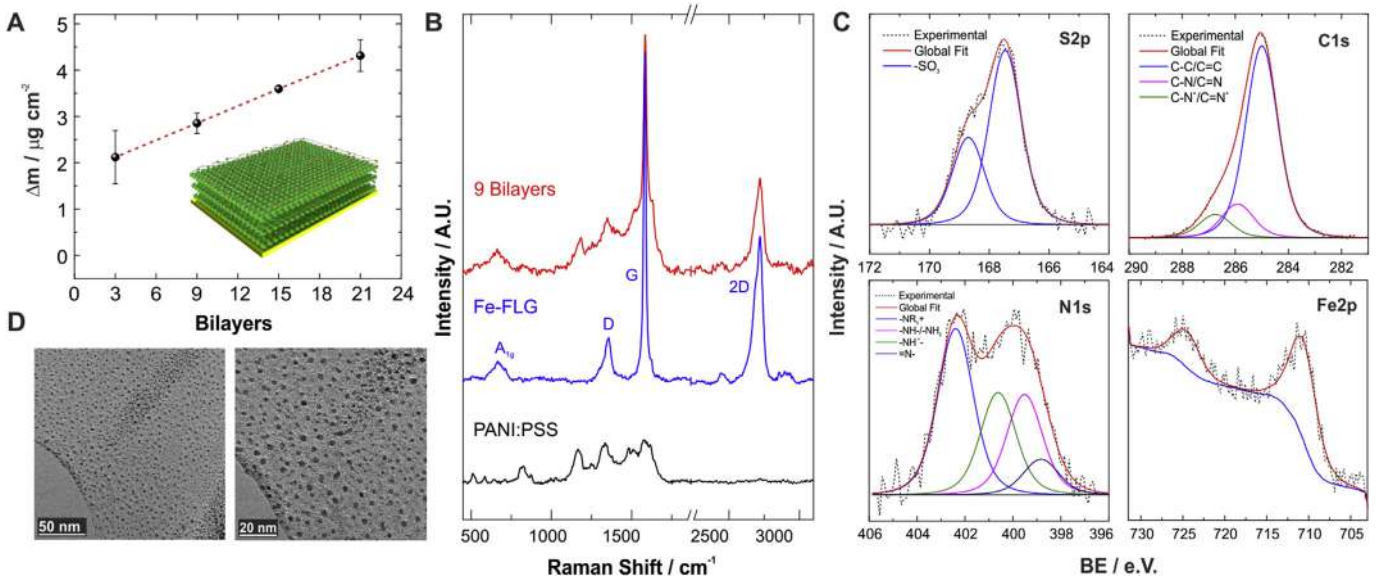

Fig. 3. Dry-state QCM deposited mass as increasing the number of bilayers (A), Raman spectra of PANI:PSS, Fe-FLG and 9-bilayers assembly **(B)**, S2p, C1s, N1s and Fe2p XPS spectra of a 21 bilayers assembly **(C)**, and TEM images of a 6-bilayers assembly showing the presence of iron NPs **(D)**.

0.1 M HCl (left) and neutral (0.1 M KCl, right) media for a 15 bilayers assembly are shown. Also, the cyclic voltammograms for different number of bilayers (3, 9, 15 and 21) in the same conditions are presented in Fig. S3 and Fig. S4, respectively. All the assemblies present good electroactivity in both media. The voltammograms show the typical pseudocapacitance behavior of PANI and graphene assemblies: two peaks attributed to Leucoemeraldine to Emeraldine and Emeraldine to Pernigraniline transitions in PANI (only one peak can be observed in voltammograms in acidic media because the second one is not reached in the potential range employed), with an important electrical double layer capacitance component ascribed to the Fe-FLG [18,57]. No peaks corresponding to the pseudocapacitive behavior of iron nanostructures were observed. This result is explained by the low content of iron oxide in the Fe-G (ca. 22%, see Fig. S1). It has been reported that at low loading (less than 55% approximately), no redox peaks are observed for iron-modified graphene nanostructures [18,58]. Notably, the integration of the water-dispersible PANI:PSS complex with the iron-modified graphene by the LbL technique yields an excellent performance of the whole coating in neutral medium. The good electrochemical response of PANI:PSS in neutral solutions has been attributed to the doping effect of the sulfonate groups on PANI, which stabilizes the voltammetric response [55,56]. Moreover, some authors have reported that the sulfonate groups of the PSS change the internal pH within the assembly by creating a more acidic microenvironment [31,59]. Furthermore, it is known that the conductivity of the graphene-like material is not affected by the changes in the pH, which also accounts for the good response in neutral medium [7].

For LbL assemblies, it has been reported that the successive deposition of layers can lead to a blocking in the ionic transport across the assembly if both components are not electronically well-connected [7]. The relation between the peak current and the scan rate for the 15 bilayers assembly is shown in the inset of Fig. 4(A) from 20 to 2000 mV s^{-1} in both neutral and acidic media. The linear behavior indicates that the LbL assembly provides good paths for the electrons without blocking the ionic transport, needed for charge compensation (the same feature can be observed in Fig. S5 for the assemblies with 3, 9, 15 and 21 bilayers).

Fig. 4(B) shows the different voltammograms as increasing the number of bilayers in both HCl (left) and KCl (right) solutions at 500 mV s^{-1}. The linear increase in the peak current with the number of bilayers for both media, presented in the inset, reveals a homogeneous deposition of the electroactive materials as the number of bilayers increases and ensures the good electrochemical connection between the successive layers and the metallic base electrode [7,42]. This result is in concordance with the QCM results (Fig. 3(A)).

In order to quantify the performance of the assemblies as both neutral and acidic medium supercapacitors, the specific capacitance from cyclic voltammetry measurements were computed according to the following equation (Equation (1)):

$$C_{SP} = \frac{1}{m\nu\left(V_f - V_i\right)} \int_{V_i}^{V_f} I(V)dV \quad (1)$$

where C_{SP} is the specific capacitance (F g^{-1}), m is the mass deposited onto the electrode obtained by the QCM measurements (g), v is the sweep rate (V s^{-1}), V_f and Vi are the integration potential limits (V) and I (A) is the current.

Fig. 4(C) shows the specific capacitance values at different scan rates obtained from cyclic voltammetry measurements for a 15 bilayers assembly in both media, and the same data is shown in Fig. S6 for 3, 9, 15 and 21 bilayers assemblies. In Fig. 4(D), the voltammetric capacitances at 20 mV s^{-1} are shown. The assembly with 15 bilayers shows the highest values of specific capacitance in both media, 265.2 F g^{-1} and 238.3 F g^{-1} for HCl and KCl, respectively. This result implies that the assembled film retains 90% of the acidic medium capacitance in KCl solution (this is the ratio of the capacitance in KCl solution over that in HCl solution). An average of 88 ± 10% capacitance retention in KCl medium was obtained from the whole set of results at different scan rates. This result confirms the possible use of this assembly as a neutral medium supercapacitor.

In order to evaluate the advantages of the LbL synthetic procedure, a composite-coated electrode was prepared by direct mixture of PANI:PSS and Fe-FLG components (see SI). The voltammetric response in both acidic and neutral solutions was lower

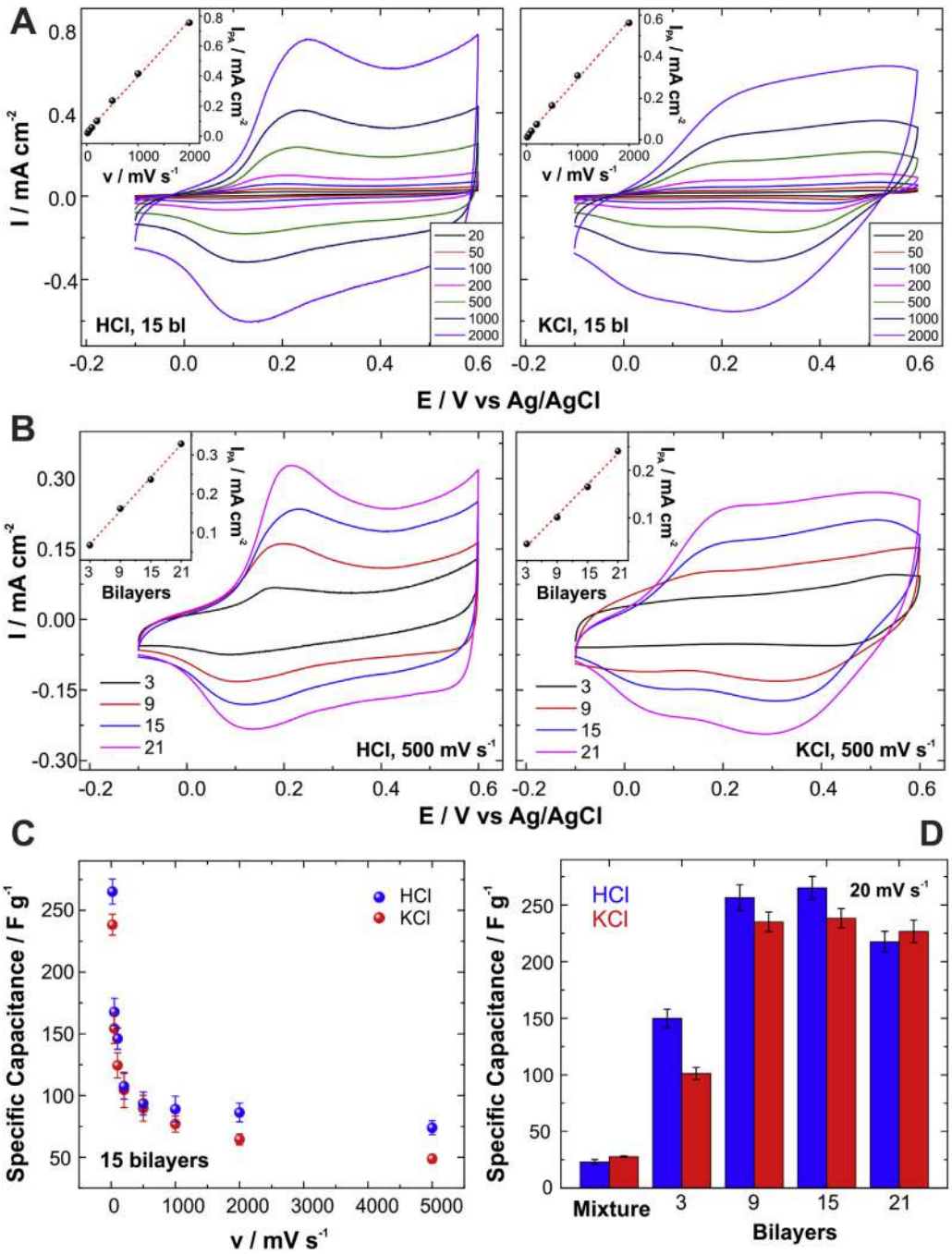

Fig. 4. Cyclic voltammograms at different scan rates in 0.1 M HCl (left) and 0.1 M KCl solutions (right) for a 15 bilayers assembly. The inset shows the anodic peak current versus the scan rate **(A)**. Cyclic voltammograms for different bilayers number in 0.1 M HCl (left) and 0.1 M KCl (right) solutions at 500 mV s^{-1}. The inset shows the anodic peak current versus the bilayers number **(B)**. Specific capacitances in HCl and KCl media obtained from the cyclic voltammetry curves for a 15 bilayers assembly **(C)**. Specific capacitances in HCl and KCl media obtained from the cyclic voltammetry curves at 20 mV s^{-1} for different bilayers number. Mixture refers to the coating formed by direct aggregation of both components **(D)**. Bars indicate SD from 5 CV curves.

and less defined than in the case of the LbL assemblies (Fig. S7). The gravimetric voltammetric capacitances at 20 mV s^{-1} were also included in Fig. 4(D). These values are significantly lower than those obtained for films produced by the LbL approach, suggesting that a high proportion of non-electroactive aggregates (or ineffective electrochemical connection between the electroactive domains and the base electrode) are produced in the case of direct mixture. These results reinforce the utility of the LbL procedure to produce well-connected electroactive materials.

In this sense, the mesostructure of the LbL assemblies was also investigated by X-ray reflectivity (XRR) (SI file). XRR results suggest higher mesoscale order in the case of the LbL assembly as compared with the coating formed by direct mixture of the components (Fig. S8). In the case of the LbL assembly, the presence of a broad Bragg peak suggests the presence of lamellar structures oriented parallel to the substrate, which were confirmed by GISAXS measurements (Fig. S9), as expected from an LbL construction strategy.

In order to further characterize the supercapacitor performance

of the assemblies, the galvanostatic charge-discharge curves at different current densities (from 1 to 5 A g^{-1}) were evaluated. The charge-discharge curves for (A) HCl and (B) KCl media are presented in Fig. 5. The galvanostatic charge-discharge curves are not linear in the whole range of potential, varying the slope during the charge/discharge. This feature has been assigned to the redox transitions in the conducting polymer [60].

The specific capacitance from the charge-discharge curves was calculated according to the following equation (Equation (2)):

$$C_{SP} = I\Delta t/(V\, m) \quad (2)$$

where C_{SP} is the specific capacitance (F g^{-1}), I (A) is the discharge current, Δt is the discharge time, V is the potential window and m is the mass deposited onto the electrode obtained from the QCM measurements (g).

The discharge C_{SP} values obtained for the 15 bilayers assembly in both acidic and neutral media are shown in Fig. 5 (C). The assembly displays specific capacitance values ranging from 768.6 F g^{-1} to 171.5 F g^{-1} and 659.2 F g^{-1} to 128.6 F g^{-1} (1–5 A g^{-1}) in HCl and KCl solutions, respectively. As noted above, the highest values were 768.6 F g^{-1} and 659.2 F g^{-1} for the current density of 1 A g^{-1}. This result implies 86% capacitance retention in neutral medium with respect to the acidic medium. From all the curves performed, we obtained an average capacitance retention in KCl medium of 82 ± 4%, which is in good agreement with the cyclic voltammetry measurements.

Furthermore, the cycling stability (at 3 A g^{-1}) was measured for the 15 bilayers assembly, the one that showed the highest specific capacitance in both media (Fig. 5 (D)). This assembled film showed 84% capacitance retention in HCl and 86% capacitance retention in KCl up to 1600 cycles. This good stability in both media can be explained by the effect of the iron-modified graphene in the assembly. The poor stability of PANI-like conducting polymers through cycling is well-documented, as well as the very good one of the graphene-like materials [18,57,60].

For comparison, some quantitative results from works on similar systems in neutral and acidic electrolytes are shown in Table 1. The assembled material developed in this work shows higher specific capacitance in both media and also good cycling stability (it is important to note here that all the results listed in this table were performed in a three-electrode cell configuration, so making the studies comparable between them).

In Fig. 6, the Ragone plot with the performance of the 15 bilayers assembly in both media is shown. The values of specific energy and specific power were calculated from the galvanostatic charge-discharge curves in the range 1–5 A g^{-1} according to the following expressions (Equation (3) and Equation (4)):

$$E = \frac{1}{2}\, C_{SP}\, V^2 \quad (3)$$

$$P = \frac{E}{\Delta t} \quad (4)$$

where E is the specific energy (W h kg-*1*), C_{SP} is the specific capacitance (F g^{-1}), V is the potential window (V), P is the specific power (W kg^{-1}) and Δt is the discharge time (seconds).

For HCl and KCl solutions, the highest specific energy reaches 52.3 W h kg^{-1} and 44.9 W h kg^{-1} at the power density of 350 W kg^{-1}, respectively. Furthermore, at the power density of 1750 W kg^{-1}, the system holds an energy density of 11.7 W h kg^{-1}

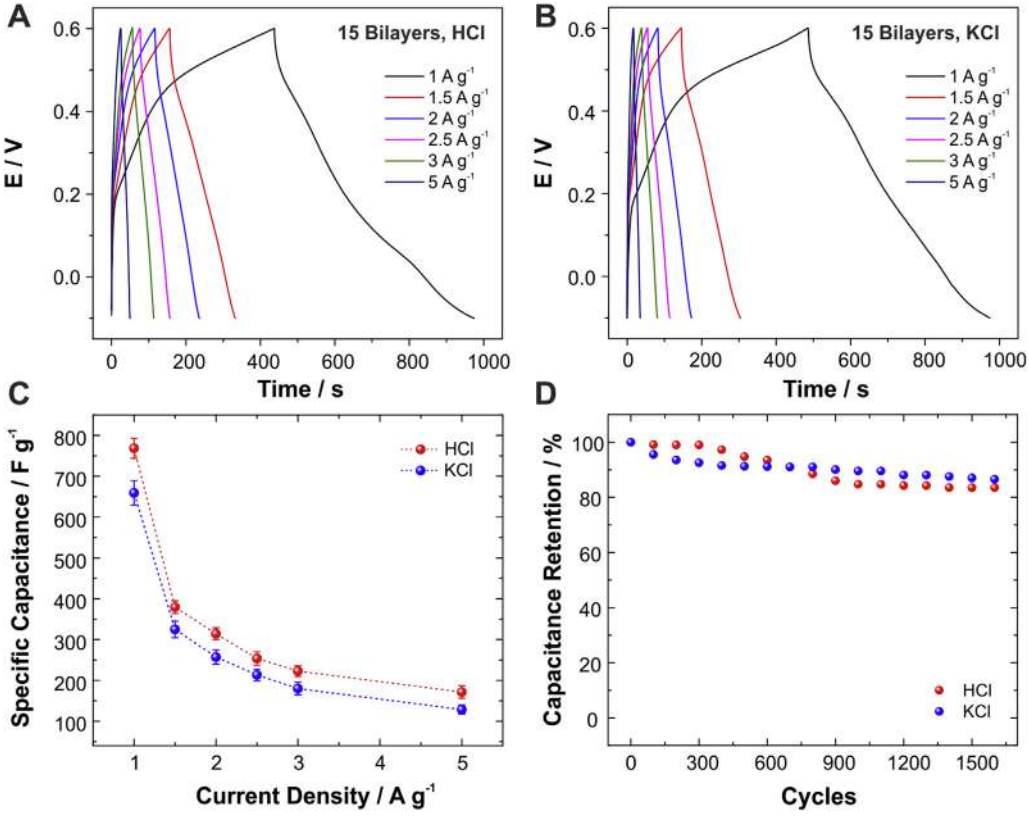

Fig. 5. Charge-discharge curves for a 15 bilayers assembly at different current densities in **(A)** 0.1 M HCl and **(B)** 0.1 M KCl. Specific capacitance values obtained from discharge curves at different current densities for a 15 bilayers assembly in both media (bars indicate SD from 5 curves for the same electrode) **(C)**. Cycling stability of the 15 bilayers assembly in both media at 3 A g^{-1} **(D)**.

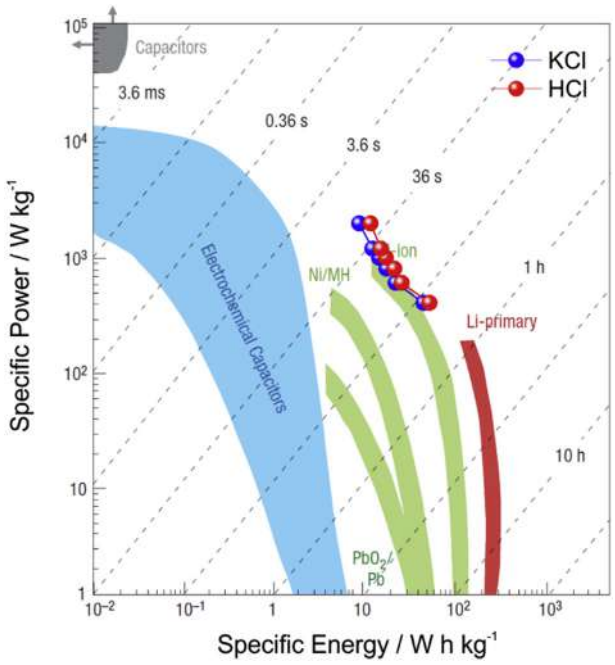

Fig. 6. Ragone plot showing the performance of the 15 bilayers assembly in both media. The figure was created by incorporating our experimental data (blue and red dots) in the Ragone plot already reported by Simon and Gogotsi. Reproduced with permission from P. Simon and Y. Gogotsi, *Nature Materials* **2008**, 7, 845. Copyright 2008 Springer Nature. (For interpretation of the references to colour in this figure legend, the reader is referred to the Web version of this article.)

and 8.75 W h kg^{-1} for acidic and neutral medium, respectively.

4. Conclusions

We presented the construction, characterization and capacitance performance of a layer-by-layer assembly of PANI:PSS complexes and Fe oxide nanoparticles-coated FLG from aqueous dispersions. The simple dip-coating procedure yielded a mechanically and electrochemically stable electrode material, which showed excellent capacitive performance in neutral aqueous electrolyte. Raman and XPS spectroscopies proved the effective incorporation of both materials, and the linear increase of the capacitance on the deposited mass proved an efficient electrochemical connection within the film. The electrochemical performance of the film-coated electrodes was tested in both acidic and neutral aqueous electrolytes, showing the best results for the 15 bilayers assembly. This assembly showed a high capacitance of 768.6 F g^{-1} and 659.2 F g^{-1} in 0.1 M HCl and 0.1 M KCl, respectively, at the current density of 1 A g^{-1}, which implies that the capacitance is not greatly diminished from acidic to neutral medium. Moreover, the system showed a good stability to continuous cycling in both media after 1600 charge-discharge cycles at 3 A g^{-1} (84% and 86% in acidic and neutral solutions, respectively). The electrode material performance is relatively high in both media, compared to similar systems reported in literature. This ternary composite coating then constitutes a promising candidate for the construction of environmentally friendly supercapacitors.

Acknowledgements

The authors acknowledge financial support from ANPCyT (PICT-2013-0905, PICT-2015-0239, PICT 2016-1680), Universidad Nacional de La Plata (PPID-X016), CONICET (PIP 0370), the Austrian Institute of Technology GmbH (AIT–CONICET Partner Lab: *"Exploratory Research for Advanced Technologies in Supramolecular Materials Science"* – Exp. 4947/11, Res. No. 3911, 28-12-2011) and the Marie Curie project "Hierarchical functionalization and assembly of graphene for multiple device fabrication" (HiGRAPHEN) (Grant ref: 612704). WAM and OA are CONICET staff members. GEF gratefully acknowledges a Doctoral Scholarship from CONICET.

Appendix A. Supplementary data

Supplementary data related to this article can be found at https://doi.org/10.1016/j.electacta.2018.07.085.

References

[1] M. Aono, K. Ariga, The way to nanoarchitectonics and the way of nanoarchitectonics, Adv. Mater. 28 (2016) 989–992.
[2] K. Ariga, Q. Ji, W. Nakanishi, J.P. Hill, M. Aono, Nanoarchitectonics: a new materials horizon for nanotechnology, Mater. Horiz. 2 (2015) 406–413.
[3] K. Ariga, Y. Yamauchi, M. Aono, Commentary: nanoarchitectonics— think about nano again, APL Mater. 3 (2015), 061001.
[4] A.H. Khan, S. Ghosh, B. Pradhan, A. Dalui, L.K. Shrestha, S. Acharya, et al., Two-Dimensional (2D) nanomaterials towards electrochemical nanoarchitectonics in energy-related applications, Bull. Chem. Soc. Jpn. 90 (2017) 627–648.
[5] J. Kim, J.H. Kim, K. Ariga, Redox-active polymers for energy storage nanoarchitectonics, Joule 1 (2017) 739–768.
[6] J. Luo, R. Liu, X. Liu, Layer-by-layer assembled ionic-liquid functionalized graphene/polyaniline nanocomposite with enhanced electrochemical sensing properties, J. Mater. Chem. C. 2 (2014) 4818–4827.
[7] W.A. Marmisollé, O. Azzaroni, Recent developments in the layer-by-layer assembly of polyaniline and carbon nanomaterials for energy storage and sensing applications. From synthetic aspects to structural and functional characterization, Nanoscale 8 (2016) 9890–9918.
[8] B.E. Conway, Electrochemical Supercapacitors: Scientific Fundamentals and Technological Applications, Springer, 1999.
[9] Y.G. Majid Beidaghi, Capacitive energy storage in micro-scale devices: recent advances in design and fabrication of micro- supercapacitors, Energy Environ. Sci. 7 (2014) 867–884.
[10] C. Zhong, Y. Deng, W. Hu, J. Qiao, L. Zhang, J. Zhang, A review of electrolyte materials and compositions for electrochemical supercapacitors, Chem. Soc. Rev. 44 (2015) 7484–7539.
[11] Z. Chang, Y. Yang, M. Li, X. Wang, Y. Wu, Green energy storage chemistries based on neutral aqueous electrolytes, J. Mater. Chem. A. 2 (2014) 10739–10755.
[12] J.L. Delgado, M. Herranz, N. Martín, The nano-forms of carbon, J. Mater. Chem. 18 (2008) 1417–1426.
[13] D. Jariwala, V.K. Sangwan, L.J. Lauhon, T.J. Marks, M.C. Hersam, Carbon nanomaterials for electronics, optoelectronics, photovoltaics, and sensing, Chem. Soc. Rev. 42 (2013) 2824–2860.
[14] S.K. Vashist, D. Zheng, K. Al-Rubeaan, J.H.T. Luong, F. Sheu, Advances in carbon nanotube based electrochemical sensors for bioanalytical applications, Biotechnol. Adv. 29 (2011) 169–188.
[15] T. Lee, S.H. Min, M. Gu, Y.K. Jung, W. Lee, J.U. Lee, et al., Layer-by-Layer assembly for graphene-based multilayer nanocomposites: synthesis and applications, Chem. Mater. 27 (2015) 3785–3796.
[16] C. Soldano, A. Mahmood, E. Dujardin, Production, properties and potential of graphene, Carbon N. Y. 48 (2010) 2127–2150.
[17] A.K. Das, S. Sahoo, P. Arunachalam, S. Zhang, J.-J. Shim, Facile synthesis of Fe_3O_4 nanorod decorated reduced graphene oxide (RGO) for supercapacitor application, RSC Adv. 6 (2016) 107057–107064.
[18] R. Kumar, R.K. Singh, A.R. Vaz, R. Savu, S.A. Moshkalev, Self-assembled and one-step synthesis of interconnected 3D network of Fe3O4/Reduced graphene oxide nanosheets hybrid for high-performance supercapacitor electrode, ACS Appl. Mater. Interfaces 9 (2017) 8880–8890.
[19] G. Inzelt, Rise and rise of conducting polymers, J. Solid State Electrochem. 15 (2011) 1711–1718.
[20] G. Inzelt, Conducting Polymers: a New Era in Electrochemsitry, second ed., Springer-Verlag, Berlin Heidelberg, 2012.
[21] J. Heinze, B.A. Frontana-Uribe, S. Ludwigs, Electrochemistry of conducting polymers-persistent models and new concepts, Chem. Rev. 110 (2010) 4724–4771.
[22] N.A. Kumar, J.-B. Baek, Electrochemical supercapacitors from conducting polyaniline-graphene platforms, Chem. Commun. 50 (2014) 6298–6308.
[23] Z. Gao, W. Yang, J. Wang, H. Yan, Y. Yao, J. Ma, et al., Electrochemical synthesis of layer-by-layer reduced graphene oxide sheets/polyaniline nanofibers composite and its electrochemical performance, Electrochim. Acta 91 (2013) 185–194.
[24] A.K. Sarker, J.D. Hong, Layer-by-Layer self-assembled multilayer films composed of graphene/polyaniline bilayers: high-Energy electrode materials for supercapacitors, Langmuir 28 (2012) 12637–12646.

[25] Q. Wu, Y. Xu, Z. Yao, A. Liu, G. Shi, Supercapacitors based on flexible graphene/polyaniline nanofiber composite films, ACS Nano 4 (2010) 1963–1970.
[26] J. Xu, K. Wang, S.Z. Zu, B.H. Han, Z. Wei, Hierarchical nanocomposites of polyaniline nanowire arrays on graphene oxide sheets with synergistic effect for energy storage, ACS Nano 4 (2010) 5019–5026.
[27] K. Zhang, L.L. Zhang, X.S. Zhao, J. Wu, Graphene/polyaniline nanofiber composites as supercapacitor electrodes, Chem. Mater. 22 (2010) 1392–1401.
[28] J. Lu, W. Liu, H. Ling, J. Kong, G. Ding, D. Zhou, et al., Layer-by-layer assembled sulfonated-graphene/polyaniline nanocomposite films: enhanced electrical and ionic conductivities, and electrochromic properties, RSC Adv. 2 (2012) 10537–10543.
[29] J. Liu, S. Tian, W. Knoll, Properties of polyaniline/carbon nanotube multilayer films in neutral solution and their application for stable low-potential detection of reduced beta-nicotinamide adenine dinucleotide, Langmuir 21 (2005) 5596–5599.
[30] Z. Hu, J. Xu, Y. Tian, R. Peng, Y. Xian, Q. Ran, et al., Layer-by-layer assembly of poly (sodium 4-styrenesulfonate) wrapped multiwalled carbon nanotubes with polyaniline nanofibers and its electrochemistry, Carbon N. Y. 48 (2010) 3729–3736.
[31] J. Luo, Y. Chen, Q. Ma, R. Liu, X. Liu, Layer-by-layer self-assembled hybrid multilayer films based on poly(sodium 4-styrenesulfonate) stabilized graphene with polyaniline and their electrochemical sensing properties, RSC Adv. 3 (2013), 17866–17673.
[32] M.M. Islam, S.H. Aboutalebi, D. Cardillo, H.K. Liu, K. Konstantinov, S.X. Dou, Self-assembled multifunctional hybrids: toward developing high-performance graphene-based architectures for energy storage devices, ACS Cent. Sci. 1 (2015) 206–216.
[33] N. Ashok Kumar, J. Baek, Electrochemical supercapacitors from conducting polyaniline–graphene platforms, Chem. Commun. 50 (2014) 6298–6308.
[34] Y. Wang, C.C. Mayorga-Martinez, M. Pumera, Polyaniline/mos X supercapacitor by electrodeposition, Bull. Chem. Soc. Jpn. 90 (2017) 847–853.
[35] H. Wang, D. Chao, J. Liu, J. Lin, Z.X. Shen, Nanoengineering of 2D tin sulfide nanoflake arrays incorporated on polyaniline nanofibers with boosted capacitive behavior, 2D Mater. 5 (2018), 031005.
[36] S.K. Simotwo, V. Kalra, Polyaniline-carbon based binder-free asymmetric supercapacitor in neutral aqueous electrolyte, Electrochim. Acta 268 (2018) 131–138.
[37] E. Pardieu, S. Pronkin, M. Dolci, T. Dintzer, B.P. Pichon, D. Begin, et al., Hybrid layer-by-layer composites based on a conducting polyelectrolyte and Fe 3 O 4 nanostructures grafted onto graphene for supercapacitor application, J. Mater. Chem. A. 3 (2015) 22877–22885.
[38] H. Li, Y. He, V. Pavlinek, Q. Cheng, P. Saha, C. Li, MnO $_2$ nanoflake/polyaniline nanorod hybrid nanostructures on graphene paper for high-performance flexible supercapacitor electrodes, J. Mater. Chem. A. 3 (2015) 17165–17171.
[39] M.M. Mezgebe, Z. Yan, G. Wei, S. Gong, F. Zhang, S. Guang, et al., 3D graphene-Fe 3 O 4 -polyaniline, a novel ternary composite for supercapacitor electrodes with improved electrochemical properties, Mater. Today Energy 5 (2017) 164–172.
[40] S. Mondal, U. Rana, S. Malik, Reduced graphene oxide/Fe3O4/polyaniline nanostructures as electrode materials for an all-solid-state hybrid supercapacitor, J. Phys. Chem. C 121 (2017) 7573–7583.
[41] T.J. Daou, G. Pourroy, S. Bégin-Colin, J.M. Grenèche, C. Ulhaq-Bouillet, P. Legaré, et al., Hydrothermal synthesis of monodisperse magnetite nanoparticles, Chem. Mater. 18 (2006) 4399–4404.
[42] G.E. Fenoy, E. Maza, E. Zelaya, W.A. Marmisollé, O. Azzaroni, Layer-by-layer assemblies of highly connected polyelectrolyte capped-Pt nanoparticles for electrocatalysis of hydrogen evolution reaction, Appl. Surf. Sci. 416 (2017) 24–32.
[43] W. Baaziz, L. Truong-Phuoc, C. Duong-Viet, G. Melinte, I. Janowska, V. Papaefthimiou, et al., Few layer graphene decorated with homogeneous magnetic Fe3O4 nanoparticles with tunable covering densities, J. Mater. Chem. A. 2 (2014) 2690.
[44] C. Wells, O. Vollin-Bringel, V. Fiegel, S. Harlepp, B. Van der Schueren, S. Bégin-Colin, et al., Engineering of mesoporous silica coated carbon-based materials optimized for an ultrahigh doxorubicin payload and a drug release activated by pH, *t* , and NIR-light, Adv. Funct. Mater. (2018), 1706996.
[45] A.C.C. Ferrari, D.M.M. Basko, Raman spectroscopy as a versatile tool for studying the properties of graphene, Nat. Nanotechnol. 8 (2013) 235–246.
[46] L. Ren, S. Huang, W. Fan, T. Liu, One-step preparation of hierarchical superparamagnetic iron oxide/graphene composites via hydrothermal method, Appl. Surf. Sci. 258 (2011) 1132–1138.
[47] O.N. Shebanova, P. Lazor, Raman study of magnetite (Fe3O4): laser-induced thermal effects and oxidation, J. Raman Spectrosc. 34 (2003) 845–852.
[48] O.N. Shebanova, P. Lazor, Raman spectroscopic study of magnetite (FeFe2O4): a new assignment for the vibrational spectrum, J. Solid State Chem. 174 (2003) 424–430.
[49] C. Yang, L. Zhang, N. Hu, Z. Yang, H. Wei, Z.J. Xu, et al., Densely-packed graphene/conducting polymer nanoparticle papers for high-volumetric-performance flexible all-solid-state supercapacitors, Appl. Surf. Sci. 379 (2016) 206–212.
[50] S. Cho, J.S. Lee, J. Jun, S.G. Kim, J. Jang, Fabrication of water-dispersible and highly conductive PSS-doped PANI/graphene nanocomposites using a high-molecular weight PSS dopant and their application in H $_2$ S detection, Nanoscale 6 (2014) 15181–15195.
[51] J.-W. Jeon, S.R. Kwon, J.L. Lutkenhaus, Polyaniline nanofiber/electrochemically reduced graphene oxide layer-by-layer electrodes for electrochemical energy storage, J. Mater. Chem. A. 3 (2015) 3757–3767.
[52] X. Peng, L. Meng, W. Zhang, W. Liu, L. Zhang, Y. Zhang, Facile preparation of nitrogen-doped graphene scrolls via acoustic cavitation as electrocatalyst for glucose biosensing, J. Solid State Electrochem. 20 (2016) 439–447.
[53] W.A. Marmisollé, D. Gregurec, S. Moya, O. Azzaroni, Polyanilines with pendant amino groups as electrochemically active copolymers at neutral pH, ChemElectroChem 2 (2015) 2011–2019.
[54] T. Fujii, F.M.F. de Groot, G. a Sawatzky, F.C. Voogt, T. Hibma, K. Okada, In situ XPS analysis of various iron oxide films grown by NO 2 -assisted molecular-beam epitaxy, Phys. Rev. B 59 (1999) 3195–3202.
[55] A.M. Bonastre, M. Sosna, P.N. Bartlett, An analysis of the kinetics of oxidation of ascorbate at poly(aniline)-poly(styrene sulfonate) modified microelectrodes, Phys. Chem. Chem. Phys. 13 (2011) 5365–5372.
[56] P.N. Bartlett, E.N.K. Wallace, The oxidation of ascorbate at poly(aniline)–poly(vinylsulfonate) composite coated electrodes, Phys. Chem. Chem. Phys. 3 (2001) 1491–1496.
[57] A. Eftekhari, L. Li, Y. Yang, Polyaniline supercapacitors, J. Power Sources 347 (2017) 86–107.
[58] J.P. Cheng, Q.L. Shou, J.S. Wu, F. Liu, V.P. Dravid, X.B. Zhang, Influence of component content on the capacitance of magnetite/reduced graphene oxide composite, J. Electroanal. Chem. 698 (2013) 1–8.
[59] J. Luo, S. Jiang, R. Liu, Y. Zhang, X. Liu, Synthesis of water dispersible polyaniline/poly(styrenesulfonic acid) modified graphene composite and its electrochemical properties, Electrochim. Acta 96 (2013) 103–109.
[60] V. Khomenko, E. Frackowiak, F. Béguin, Determination of the specific capacitance of conducting polymer/nanotubes composite electrodes using different cell configurations, Electrochim. Acta 50 (2005) 2499–2506.
[61] W.H. Khoh, J.D. Hong, Layer-by-layer self-assembly of ultrathin multilayer films composed of magnetite/reduced graphene oxide bilayers for supercapacitor application, Colloids Surfaces A Physicochem. Eng. Asp. 436 (2013) 104–112.
[62] M. Ammam, J. Fransaer, Performance of SLS/MWCNTs/PANI capacitor electrodes in a physiological electrolyte and in serum, Chem. Commun. 48 (2012) 2036.
[63] H. Wang, D. Chao, J. Liu, J. Lin, Z.X. Shen, Nanoengineering of 2D tin sulfide nanoflake arrays incorporated on polyaniline nanofibers with boosted capacitive behavior, 2D Mater. 5 (2018), 031005.
[64] H. Mi, X. Zhang, X. Ye, S. Yang, Preparation and enhanced capacitance of core–shell polypyrrole/polyaniline composite electrode for supercapacitors, J. Power Sources 176 (2008) 403–409.
[65] T. Lee, T. Yun, B. Park, B. Sharma, H.-K. Song, B.-S. Kim, Hybrid multilayer thin film supercapacitor of graphene nanosheets with polyaniline: importance of establishing intimate electronic contact through nanoscale blending, J. Mater. Chem. 22 (2012) 21092.
[66] J. Luo, Q. Ma, H. Gu, Y. Zheng, X. Liu, Three-dimensional graphene-polyaniline hybrid hollow spheres by layer-by-layer assembly for application in supercapacitor, Electrochim. Acta 173 (2015) 184–192.
[67] S. Mondal, U. Rana, S. Malik, Reduced graphene Oxide/Fe $_3$ O $_4$/polyaniline nanostructures as electrode materials for an all-solid-state hybrid supercapacitor, J. Phys. Chem. C 121 (2017) 7573–7583.